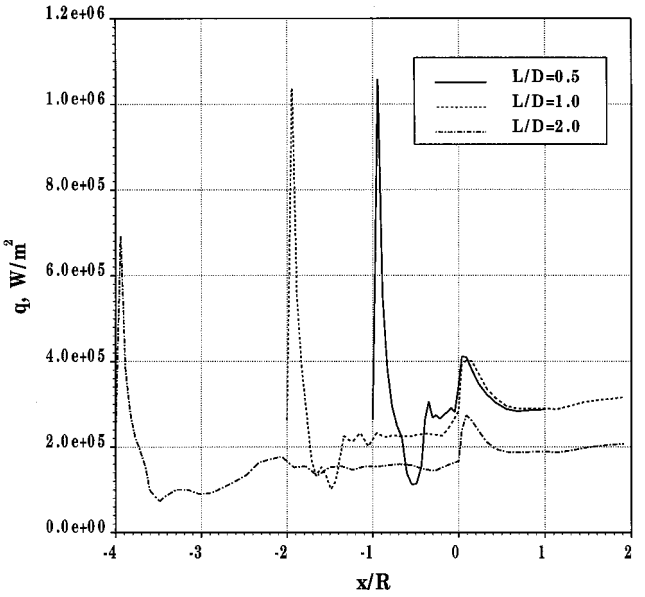

Fig. 6 Variation of wall heat flux.

Crawford[5] at $L/D = 2.0$ is found to be about 20%. The accuracy of the measured data is not available.

Figures 5 and 6 show the computed variation of surface skin-friction coefficient Cf and wall heat flux q along the spike blunt body. Negative skin friction can be seen on the spike, which is due to flow separation. The separation zone is found to be a function of the spike length. A sharp and sudden rise of skin friction and heat transfer is found very close to the spike tip, which is due to flow stagnation. The secondary peak heat flux is observed at about the reattachment point. This secondary peak heat flux decreases with increasing spike length.

Conclusions

The flowfield around a forward facing spike attached to a hemisphere–cylinder nosetip has been calculated at a freestream Mach number of 6.8 for different spike lengths. The flow features around the spiked blunt body are characterized by a conical shock wave emanating from the spike tip, a separated region in front of the blunt body, and the resulting reattachment shock wave for various freestream Mach numbers. The peak in local pressure and the heat flux are observed on the blunt-body region at the same position. The shear layer created by the spike passes through the reattachment shock wave giving the peak wall pressure and heat flux on the blunt body, which is influenced by the conical–shock reattachment interaction.

Acknowledgments

The author wishes to express his gratitude to the journal editors and reviewers for giving valuable suggestions toward the improvement of the present Note.

References

[1]Reding, J. P., Guenther, R. A., and Richter, B. J., "Unsteady Aerodynamic Considerations in the Design of a Drag-Reduction Spike," *Journal of Spacecraft and Rockets*, Vol. 14, No. 1, 1977, pp. 54–60.

[2]Stadler, J. R., and Nielsen, H. V., "Heat Transfer from a Hemisphere-Cylinder Equipped with Flow-Separation Spikes," NACA TN 3287, Sept. 1954.

[3]Bogdonoff, S. M., and Vas, I. E., "Preliminary Investigations of Spiked Bodies at Hypersonic Speeds," *Journal of the Aerospace Sciences*, Vol. 26, No. 2, 1959, pp. 65–74.

[4]Chapman, D. R., "A Theoretical Analysis of Heat Transfer in Region of Separated Flow," NACA TN 3792, June 1956.

[5]Crawford, D. H., "Investigation of the Flow over a Spiked-Nose Hemisphere Cylinder at a Mach Number of 6.8," NASA TN D-118, Dec. 1959.

[6]Maull, D. J., "Hypersonic Flow over Axially Symmetric Spiked Bodies," *Journal of Fluid Mechanics*, Vol. 8, Pt. 4, 1960, pp. 584–592.

[7]Wood, C. J., "Hypersonic Flow over Spiked Cones," *Journal of Fluid Mechanics*, Vol. 12, Pt. 4, 1962, pp. 614–627.

[8]Guenther, R. A., and Reding, J. P., "Fluctuating Pressure Environment of a Drag Reduction Spike," *Journal of Spacecraft and Rockets*, Vol. 14, No. 12, 1977, pp. 705–710.

[9]Yamauchi, M., Fujii, K., Tamura, Y., and Higashino, F., "Numerical Investigation of Supersonic Flows Around a Spiked Blunt Body," AIAA Paper 93-0887, Jan. 1993.

[10]Peyret, R., and Vivind, H., *Computational Methods for Fluid Flow*, Springer-Verlag, Berlin, 1993, pp. 109–111.

[11]Jameson, A., Schmidt, W., and Turkel, E., "Numerical Solution of Euler Equations by Finite Volume Methods Using Runge–Kutta Time Stepping Schemes," AIAA Paper 81-1259, June 1981.

[12]Mehta, R. C., "Numerical Investigation of Viscous Flow over a Hemisphere-Cylinder," *Acta Mechanica*, Vol. 128, No. 1–2, 1998, pp. 48–58.

[13]Shang, J. S., "Numerical Simulation of Wing-Fuselage Aerodynamic Interference," *AIAA Journal*, Vol. 22, No. 10, 1984, pp. 1345–1353.

M. Torres
Associate Editor

Boat Tail Effect of a Payload Fairing on the Elastic Displacement Response

V. Ramamurti*
Indian Institute of Technology, Chennai 600 036, India
and
S. Rajarajan† and G. V. Rao‡
Vikram Sarabhai Space Center, Trivandrum 695 022, India

Nomenclature

$[C]$	=	damping matrix
$[D_p]$, $[D_f]$	=	in-plane and bending stress–strain matrix
E	=	Young's modulus
$f(t)$	=	forcing function
h	=	thickness of the plate
$[K]$	=	assembled global stiffness matrix
$L1, L2, L3$	=	area coordinates
$[M]$	=	assembled global mass matrix
$\{u, v, w\}$	=	nodal displacements
α, β	=	constants
$\{\delta_p\}$, $\{\delta_f\}$	=	in-plane and bending nodal displacement vector
$\{\varepsilon\}$	=	total strain
$\{\varepsilon_p\}$, $\{\varepsilon_f\}$	=	in-plane and bending strain
$\{\theta_x, \theta_y, \theta_z\}$	=	nodal rotations of plate and shell element
υ	=	Poisson's ratio
ϕ, φ, θ	=	nodal rotations of beam elements
ω	=	natural frequency, rad/s

Introduction

THE main structural purpose of the payload fairing in any launch vehicle is to protect the payload from aerodynamic loading, heating, acoustic vibration, and other environmental conditions during the ascent phase and to provide an aerodynamic forward surface. The payload fairing is no longer required once the vehicle clears the atmosphere. Hence, it is jettisoned as soon as its purpose is served, to save weight and to allow for the separation of the satellite. A payload fairing is made in two or more sectors. The Atlas fairing is made in two 180-deg halves, and explosive bolts are used to begin separation. Spring-loaded actuators at the top of the cone section push the halves apart, while the aft end of each fairing half begins to rotate on hinges on a structure called the stub adaptor.[1] The Japanese H-ll rocket satellite fairing is also made in two halves, and

Received 8 November 1999; revision received 24 March 2000; accepted for publication 5 May 2000.

*Professor, Machine Dynamics Laboratory.
†Engineer, Launch Vehicle Design Group.
‡Group Director, Structural Engineering Group.

pyrotechnic is used for the separation.[2] The Titan 4 payload fairing (25.8 m long) is constructed in trisectors and uses, along the longitudinal edges, a Nomex covered elastomeric bellows that contains the explosives to provide the separation force.[3] The indian Polar Satellite Launch Vehicle (PSLV) uses a zip-cord-based mechanism to jettison the two halves of the payload fairing.[4] The successful testing of the Titan 4 payload fairing and the analysis used to predict the structural response are described in Ref. 5. Cheng[6] presented an analytical procedure to simulate the separation dynamics based on a coupled gas/structure model validated through testing. This procedure provides an inexpensive tool for studying Titan 4 payload fairings of different lengths. The dynamics associated with the Indian PSLV is presented in Ref. 7, which explains an analytical procedure for computation of the minimum impulse needed for the safe separation of any physically realizable combination of design parameters. The significance of the elastic movements in separation studies is brought out in Ref. 8. Different configurations of payload fairing, with and without a boat tail, being used are based on the mission requirements and payload size. In this work, detailed finite element studies are carried out to study the effect of the boat tail angle of a typical payload fairing on the displacement response due to a separation force.

Payload Fairing Configuration

The payload fairing consists of the following basic structural elements: 1) boat tail, 2) cylinder, 3) nose cone and 4) nose cap. These structural members have end rings for interfacing, longitudinal/circumferential stiffeners, bulk heads, and edge beams.

Typical payload fairing configuration details and the boat tail angle θ measurement convention used in this analysis are shown in Fig. 1. The overall height and the diameter of the payload fairing structure are kept constant in the present work. The structural properties of the beam members of the fairing are given in Table 1.

Table 1 Sectional properties of beam members

Description	Area, mm^2	Moment of inertia, mm^4		
		I_{xx}	I_{yy}	I_{zz}
Nose cone forward end ring	402	61,225	97,380	3,565
Nose cone bulk head	128	11,166	33,333	119
Cylinder bulk head	757	238,782	128,553	10,390
Boat tail forward end ring	1,108	371,131	272,033	25,065
Boat tail aft end ring	1,212	664,364	160,271	41,483
Boat tail stiffeners	202	91,467	30,695	185
Nose cone aft end ring	895	293,014	136,454	12,606
Nose cap ring + nose cone forward end ring	718	201,436	155,217	5,336
Piston beam	1,362	279,300	955,800	6,865
Nose cone edge beam	1,289	469,824	608,174	3,938
Boat tail edge beam	841	91,841	374,713	7,959

Finite Element Formulation

Plate and Shell Element

A three-noded triangular plate and shell element with six degrees of freedom per node is used for modeling the shells. A typical finite element and the nodal degrees of freedom are shown in Fig. 2. The details of the formulation of this element are as follows.

The in-plane displacements are given by

$$\{\delta_p\} = [u_1 \quad v_1 \quad u_2 \quad v_2 \quad u_3 \quad v_3]^T \tag{1}$$

The bending displacements are given by

$$\{\delta_f\} = [w_1 \quad \theta_{x1} \quad \theta_{y1} \quad w_2 \quad \theta_{x2} \quad \theta_{y2} \quad w_3 \quad \theta_{x3} \quad \theta_{y3}]^T \tag{2}$$

For plate bending problems, the strains are

$$\{\varepsilon\} = \begin{Bmatrix} \varepsilon_p \\ \varepsilon_f \end{Bmatrix} \tag{3}$$

where

$$\{\varepsilon_p\} = \begin{Bmatrix} \varepsilon_x \\ \varepsilon_y \\ \gamma_{xy} \end{Bmatrix} = \begin{Bmatrix} \dfrac{\partial u}{\partial x} \\ \dfrac{\partial v}{\partial y} \\ \dfrac{\partial u}{\partial y} + \dfrac{\partial v}{\partial x} \end{Bmatrix} \tag{4}$$

$$\{\varepsilon_f\} = \begin{Bmatrix} -\dfrac{\partial^2 w}{\partial x^2} \\ -\dfrac{\partial^2 w}{\partial y^2} \\ -\dfrac{2\partial^2 w}{\partial x \partial y} \end{Bmatrix} \tag{5}$$

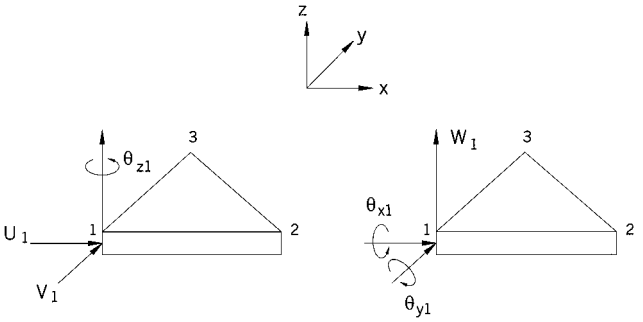

Fig. 2 Three-noded plate and shell element.

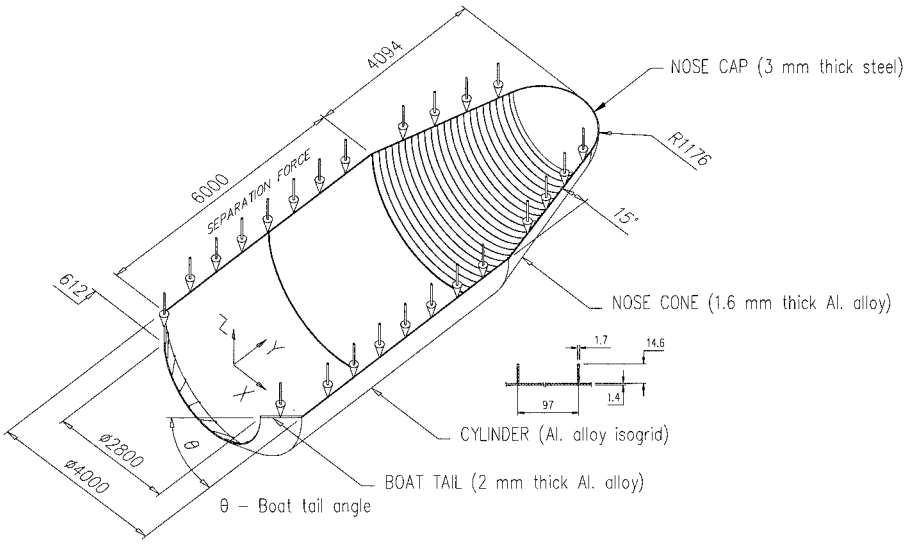

Fig. 1 Typical payload fairing configuration (one-half, for θ = 45 deg).

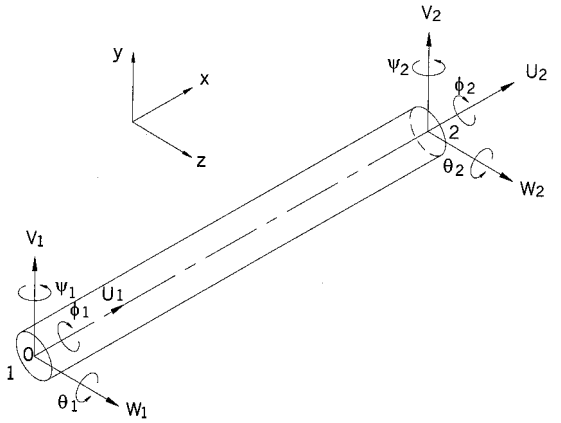

Fig. 3 Two-noded three-dimensional beam element.

The stress–strain relationship is given by

$$\{\sigma\} = [D]\{\varepsilon\} \tag{6}$$

that is,

$$\begin{Bmatrix} \sigma_p \\ \sigma_f \end{Bmatrix} = \begin{bmatrix} D_p & 0 \\ 0 & D_f \end{bmatrix} \{\varepsilon\} \tag{7}$$

where

$$[D_p] = \frac{Eh}{(1-\nu^2)} \begin{bmatrix} 1 & \nu & 0 \\ \nu & 1 & 0 \\ 0 & 0 & (1-\nu)/2 \end{bmatrix} \tag{8}$$

$$[D_f] = \frac{Eh^3}{12(1-\nu^2)} \begin{bmatrix} 1 & \nu & 0 \\ \nu & 1 & 0 \\ 0 & 0 & (1-\nu)/2 \end{bmatrix} \tag{9}$$

where σ_p is the in-plane stress resultant and σ_f is the stress due to the bending and twisting moment.

Linear polynomials for in-plane displacements u and v and cubic polynomials for bending displacements[9] w used for the shape functions are given by

$$u = \beta_1 L_1 + \beta_2 L_2 + \beta_3 L_3 \tag{10}$$

$$v = \beta_4 L_1 + \beta_5 L_2 + \beta_6 L_3 \tag{11}$$

$$\begin{aligned} w = {} & \alpha_1 L_1 + \alpha_2 L_2 + \alpha_3 L_3 + \alpha_4\left(L_2^2 L_1 + \tfrac{1}{2} L_1 L_2 L_3\right) \\ & + \alpha_5\left(L_1^2 L_2 + \tfrac{1}{2} L_1 L_2 L_3\right) + \alpha_6\left(L_3^2 L_2 + \tfrac{1}{2} L_1 L_2 L_3\right) \\ & + \alpha_7\left(L_2^2 L_3 + \tfrac{1}{2} L_1 L_2 L_3\right) + \alpha_8\left(L_3^2 L_1 + \tfrac{1}{2} L_1 L_2 L_3\right) \\ & + \alpha_9\left(L_1^2 L_3 + \tfrac{1}{2} L_1 L_2 L_3\right) \end{aligned} \tag{12}$$

Three-Dimensional Beam Element

The three-dimensional beam element with two nodes per element and six degrees of freedom with the following displacement vector is used for modeling the stiffeners, end rings, edge beams, and bulkheads:

$$\{\delta\} = [u_1 \quad v_1 \quad w_1 \quad \phi_1 \quad \varphi_1 \quad \theta_1 \quad u_2 \quad v_2 \quad w_2 \quad \phi_2 \quad \varphi_2 \quad \theta_2]^T \tag{13}$$

The element details are shown in Fig. 3.

Linear variation is used for the axial displacement and cubic polynomials for the lateral displacements.[10]

Analysis

Eigenvalue Problem

The equation of motion of a free vibration problem is given by

$$[M]\{\ddot{\delta}\} + [K]\{\delta\} = 0 \tag{14}$$

Table 2 Maximum displacements in the +ve, X direction (boat tail angle 55 deg)

Location	Displacement, mm		% Deviation
	MSC NASTRAN	Present study	
Boat tail forward end	213	203	4.7
Cylinder middle	566	535	5.5
Near cylinder top	605	572	5.5

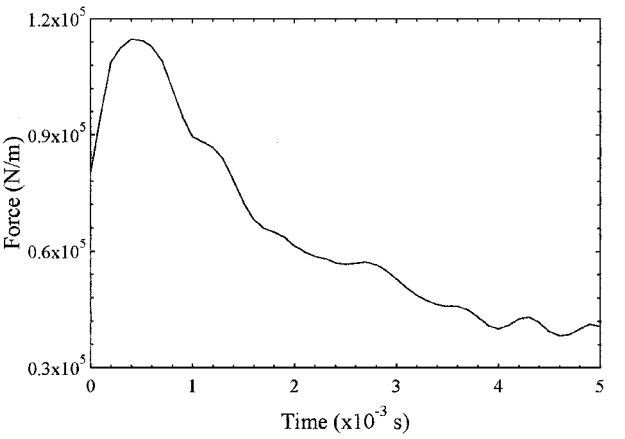

Fig. 4 Typical separation force details.

A harmonic motion of displacement in the form $\delta = \delta_0 e^{i\omega t}$ is assumed.

The Lanczos method is used to tridiagonalize the matrix, and an inverse iteration method is used[10] to solve for the lowest eigenvalues and corresponding eigenvectors.

Free–free vibration studies are carried out for the piston side of the payload fairing. The symmetry condition is made use of, and a half model of the piston side fairing is used for the analysis. The symmetry boundary condition is used at the symmetric plane. Analysis is carried out for different boat tail angles from 10 to 80 deg varying in steps of 5 deg. Additionally, a configuration without boat tail is also considered, which in effect means 0-deg boat tail angle.

Response Analysis

For a system with damping, the governing differential equation is given by

$$[M]\{\ddot{\delta}\} + [C]\{\dot{\delta}\} + [K]\{\delta\} = \{f(t)\} \tag{15}$$

Damping is assumed as 1% and constant for all of the modes.

A mode superposition technique[10] is used to decouple the equations, and they are solved for the displacement response. Separation force details given in Fig. 4 are used to determine the displacement response in X (in the direction perpendicular to the direction of force application) and Z (along the direction of force application) directions (Fig. 1) for all of the configurations. The separation forces are acting along the edges of the fairing as shown in Fig. 1.

Results and Discussion

This formulation is validated with the results obtained using the Macneal–Schwendler Corporation (MSC) NASTRAN finite element package. CTRIA3 and CBEAM elements are used for modeling the shell and beam elements. A brief outline of the comparison is presented in Table 2 for the configuration with boat tail angle 55 deg.

The first five flexible mode frequencies are plotted against different boat tail angles in Fig. 5. Frequencies increase from the configuration without boat tail to the 80-deg boat tail angle configuration. The fundamental frequency is the lowest (1.31 Hz) for the configuration without boat tail. The highest value (3.0 Hz) is for the boat tail angle of 80 deg. The first 25 elastic modes are used for the response studies.

The X direction displacement response at four critical locations along the length of the force acting edge of the fairing, namely, boat

tail aft end, boat tail forward end, cylinder middle, and near cylinder top, for boat tail angles of 10, 45, and 80 deg and the without boat tail configuration are given in Fig. 6.

Large displacements are observed in all of the boat tail configurations in the direction perpendicular to the force to the extent of 788 mm in the $+ve$ direction and 900 mm in the $-ve$ direction. For boat tail angles up to 25 deg, the maximum displacement is observed at the boat tail aft/forward end. For boat tail angles between 30 and 40 deg, the maximum displacement is at the cylinder middle, whereas for boat tail angles 45–80 deg, the maximum displacement is near the cylinder top. With the increase in boat tail angle, the displacement reduces in the boat tail structural element, indicating high local stiffness. The configuration without a boat tail displays very large elastic displacements (1206 mm) at the cylinder aft end.

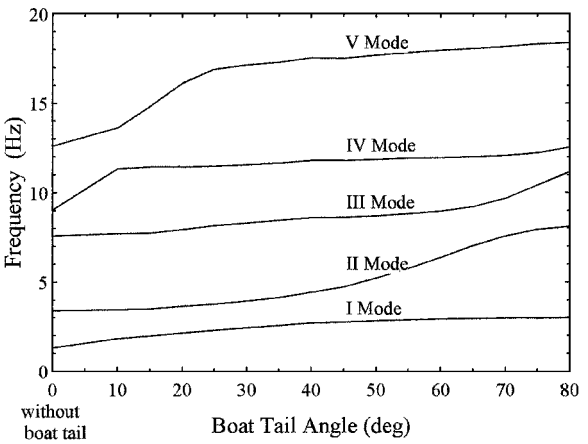

Fig. 5 Eigenvalues for different boat tail angles.

The displacements along the direction of the forces (Z direction) are much lower compared to those in the perpendicular direction. For the without boat tail configuration, the maximum displacement (369 mm) is at the cylinder aft end. For boat tail angles between 10 and 25 deg, the maximum displacement (300 mm) is at the boat tail aft/forward end, and for the rest of the cases, it is near the cylinder top. All of the configurations, other than the without boat tail case, have small initial movements in the direction opposite to the direction of the force at boat tail aft end. This tendency increases gradually from 10-deg boat tail angle to 65 deg, and thereafter it gradually reduces. When the boat tail height becomes smaller, corresponding to the increase in boat tail angle, the tendency covers a greater length of the boat tail structural element, and, for example, at an 80-deg angle, the entire boat tail starts initial movements in the direction opposite to the force direction.

Conclusions

A three-noded triangular plate and shell element and three-dimensional beam element are used for the free vibration analysis of a typical 4-m-diam payload fairing for different boat tail angles. The configuration without the boat tail is found to be very flexible compared to the configurations with a boat tail structural element. Boat tail angle has an increasing effect on the natural frequencies. A mode superposition method is used to study the effect of boat tail angle on the elastic displacement response due to a typical separation force, and the configuration without a boat tail is found to be display much larger movements compared to the configurations with boat tail. The displacements generally reduce with an increase in the boat tail angle. These studies provide very useful inputs for assessing the suitability of different boat tail configurations.

Acknowledgments

Discussions with A. Prashanthan, M. Sundaresan, K. Singa Rao, and E. Janardhana of the Launch Vehicle Design Group, Vikram Sarabhai Space Centre, Trivandrum, are thankfully acknowledged.

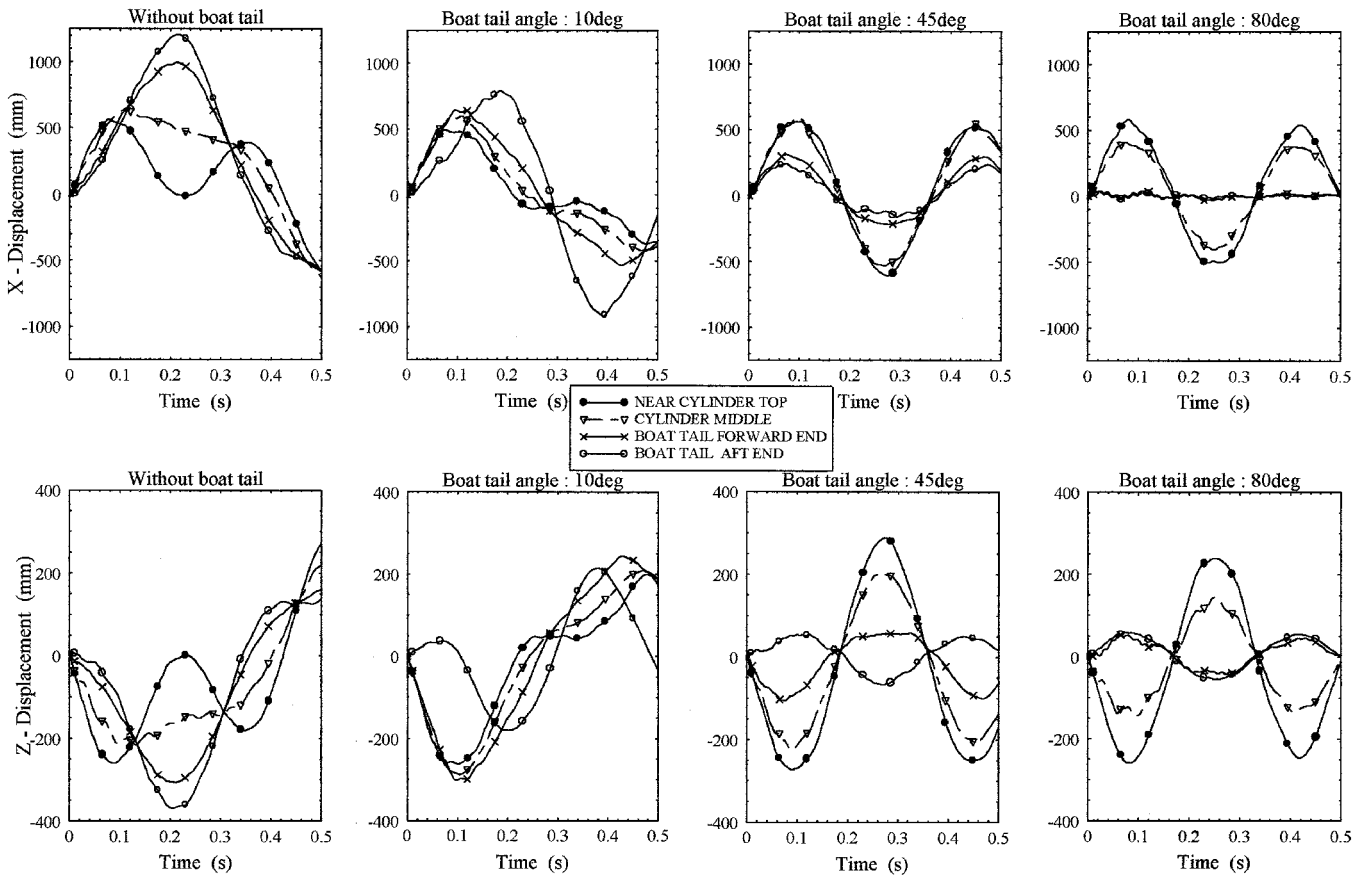

Fig. 6 Displacements in X and Z directions.

References

[1]Robbins, M. J., "Ground Test Program for New Atlas Payload fairing," *Research in Structures, Structural Dynamics and Materials*, NASA CP-3064, April 1990, pp. 194–205.

[2]Yasunaga, Y., Fukushima, Y., Nakamura, T., and Fujita, T., "Separation Jettison Test of Japanese H-ll Rocket Satellite Fairing," *Proceedings of the 28th Aerospace Sciences Meeting*, AIAA, Washington, DC, 1990, pp. 1–8.

[3]Kandebo, S. W., "Payload Capacity of Titan 4 to Expand with New Fairing," *Aviation Week and Space Technology*, 10 Dec. 1990, pp. 58–62.

[4]Anjaneyalu, M., Sudhakara Rao, K., and Srinivasan, S., "The Polar Satellite Launch Vehicle and Mission for the Indian Remote Sensing Spacecraft," International Astronautical Federation, IAF-88-168, Paris, 1988, pp. 1–8.

[5]Steinmeyer, J. F., Hofeditz, J. T., and Brierley, J. M., "Separation Testing of the Titan IV 86 ft Payload Fairing," *13th Proceedings of Aerospace Testing Seminar*, Inst. of Environmental Sciences, Manhattan Beach, CA, 1991, pp. 241–250.

[6]Cheng, S. C., "Payload Fairing Separation Dynamics," *Proceedings of the 35th Structures, Structural Dynamics, and Materials Conference*, AIAA, Washington, DC, 1994, pp. 2353–2359.

[7]Lochan, R., Adimurthy, V., and Kumar, K., "Separation Dynamics of Heatshield Fairing," *Journal of Aerospace Engineering*, Vol. 211, Pt. G, 1997, pp. 67–80.

[8]Elayuthu, M. N. G., and Abdul Salam, E. M., "Elastic Response of a Launch Vehicle Payload Fairing to Separation Shock," *Proceedings of International Conference on Finite Elements in Computational Mechanics*, Pergamon, New York, 1985, pp. 807–814.

[9]Zienkiewicz, O. C., *The Finite Element Method in Engineering Sciences*, 3rd ed., Tata McGraw–Hill, New Delhi, India, 1989, pp. 226–265, 329–353.

[10]Ramamurti, V., *Computer Aided Mechanical Design and Analysis*, Tata McGraw–Hill, New Delhi, India, 1992, pp. 7–9, 121–151, 240–248.

R. B. Malla
Associate Editor

Simulation for Deployment of an Inflatable Disk in Orbit

Kentaro Takahashi*
Mitsubishi Heavy Industries, Ltd., Yokohama 236-8515, Japan
and
Harunori Nagata† and Isao Kudo‡
Hokkaido University, Sapporo 060-8628, Japan

Introduction

A SMALL satellite is planned to be launched as a piggyback payload on a Japanese H-II vehicle to further investigate the cold-welding phenomenon that is observed when welding two metal rods together without heating in the ultrahigh-vacuum wake produced behind an orbiting spacecraft. Satellites that utilize the same concept have flown on the space shuttle several times before.[1] Because the allowable volume for the satellite is $50 \times 50 \times 50\ \text{cm}^3$ and its maximum weight is 50 kg, a 2-m-diam wake shield disk must be folded at launch and deployed in space. An inflatable tube and disk were adopted for this purpose. The advantages of an inflatable structure can be seen in the weight reduction, small packaging volume, low production cost, and high reliability of deployment compared with a conventional mechanically erectable structure.[2,3] However, at the NASA-sponsored In-Space Technology Experiment Program (In-STEP) flight experiment on the Spartan207 satellite in 1996, two supporting inflatable struts doubled during the deployment. Even if doubled tubes were finally solved by adding gas into the tube, it was indicated that care must be taken regarding the behavior of the tube during its deployment. In the case of an inflatable wake shield, its behavior must be cleared before launch. Figure 1 shows the test satellite, and Fig. 2 shows the deployment scheme of the inflatable disk. The structure is a membrane disk supported by an inflatable tube that is placed at the center of the disk extending in the radial direction and continuing around the peripheral of the disk. Before launch, the disk is folded multiple times, and it is deployed on orbit by introducing nitrogen gas into the inflatable tube, as in Fig. 2. The disk and its tube are constructed of heat-resistant polyimide resin. Because it is an extremely small outgassing material, pressure around the satellite will be below 10^{-9} Pa, and, just after the orbit insertion, the wake shield surface will be directed toward the sun to degas the sticking gas on the disk and tube. This Note describes the behavior during deployment of the inflatable disk and tube.

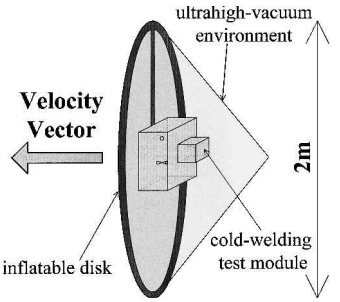

Fig. 1 Cold-welding test satellite.

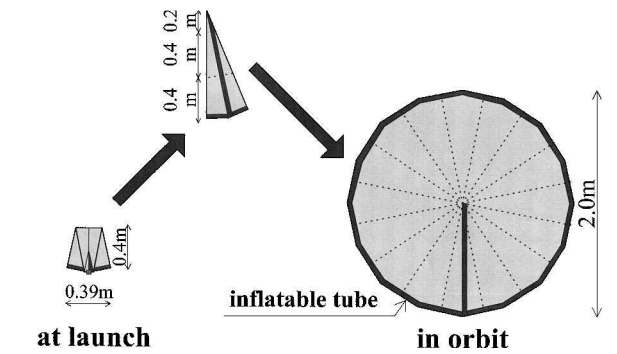

Fig. 2 Scheme of deployment of inflatable disk.

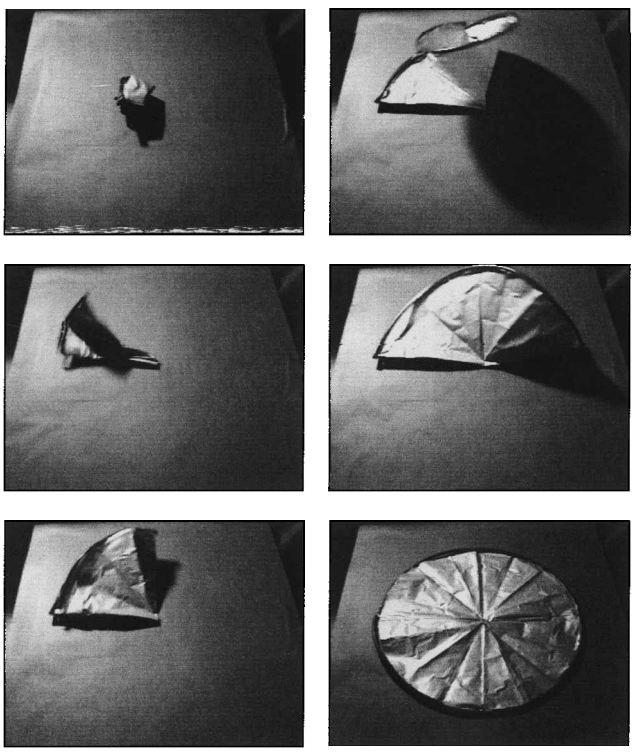

Fig. 3 Deployment of inflatable disk on floor.

Received 20 April 2000; revision received 30 June 2000; accepted for publication 15 July 2000.

*Engineer, Yokohama Works, 8-1, Sachiura, 1-chome, Kanazawa-ku.

†Assistant Professor, Faculty of Engineering, North 13, West 8, Kita-ku.

‡Professor, Faculty of Engineering, North 13, West 8, Kita-ku. Senior Member AIAA.